A Model Based Study of the Emergence of North Atlantic Deep Water during the Cenozoic: A Tale of Geological and Climatic Forcings

Erwan Pineau[1], Yannick Donnadieu[1], Pierre Maffre[2], Camille Lique[3], Thierry Huck[3], Anthony Gramoullé[1]and Jean-Baptiste Ladant[4]

[1]Centre Européen de Recherche et d'Enseignement en Géosciences de l'Environnement, Aix-en-Provence, France
[2]Géosciences Environnement Toulouse, Toulouse, France
[3]Univ Brest, CNRS, Ifremer, IRD, Laboratoire d'Océanographie Physique et Spatiale (LOPS, UMR 6523), IUEM, 29280 Plouzané, France
[4]Laboratoire des Sciences du Climat et de l'Environnement, Saclay, France

Key Points:

- Understanding the mechanisms that led to the formation of NADW during the Cenozoic
- Our simulations show a shift in ocean circulation from Southern Ocean-driven in the middle Eocene to bipolar with AMOC in the early Miocene
- Miocene paleogeography favours the NADW formation through ocean circulation and atmosphere dynamics

---

Corresponding author: Erwan Pineau, `pineau@cerege.fr`

Abstract

The North Atlantic Deep Water (NADW) is a key component of modern climate systems, redistributing heat from equatorial to polar regions and contributing to the Atlantic Meridional Overturning Circulation. However, the timing of its emergence and the mechanisms driving its formation remain uncertain. This study explores ocean circulation patterns during the middle Eocene (48–38 Ma) and early Miocene (23–16 Ma) using simulations with the IPSL-CM5A2 climate model. In the middle Eocene simulations, reduced surface salinity in the North Atlantic prevents NADW formation, regardless of atmospheric CO_2 levels or the presence of an Antarctic ice sheet. Conversely, early Miocene simulations suggest that paleogeographic shifts promote higher Atlantic salinity, enabling NADW formation. Specifically, the closure of the Polish Strait and the narrowing of the Central American Seaway enhance salt retention in the Atlantic and increase salt transport from subtropical to subpolar regions. Additionally, changes in African monsoonal precipitation—characterized by a reduction and eastward shift across Central Africa—reduce freshwater influx into the Atlantic between the middle Eocene and early Miocene. These combined factors weaken North Atlantic stratification, facilitating NADW development during the early Miocene. This research provides a timeline for NADW initiation and insights into the processes driving its formation.

1 Introduction

Large scale ocean circulation transports excess heat accumulated in tropical regions to high latitudes (Spielhagen et al., 2011). One of the main driver of this circulation is the formation of deep waters in high latitudes (Böning et al., 2006), a shift in magnitude or location of which could exert significant influence on climate dynamics, biological systems, carbon and heat ocean uptake (Lozier et al., 2008; Schmittner & Lund, 2015). Nowadays, the Atlantic Meridional Overturning Circulation (AMOC) is one of the two main cells forming the Global Meridional Overturning Circulation (GMOC) (Talley, 2013). The surface branch of the AMOC, composed of the Gulf Stream extended by the North Atlantic Current, transports warm and salty water from low to high latitudes. In some specific sites of the Labrador, Irminger and Nordic seas, these warm waters lose heat to the atmosphere, become less buoyant and subsequently sink down to 3000 m (Marshall & Schott, 1999). This results into the formation of the North Atlantic Deep Water (NADW) that feeds the deeper branch of the AMOC, flowing southward at depth toward the Southern Ocean where the Antarctic Circumpolar Current (ACC) and the westerlies upwell these water masses, closing the AMOC with the Antarctic Intermediate Water (AAIW) (Talley, 2013).

However, this GMOC configuration has evolved over the geological epochs (Ferreira et al., 2018). The Atlantic Ocean gradually formed after the break-up of the Pangaea (Granot & Dyment, 2015; Labails et al., 2010). The initiation period of the AMOC has been the topic of many paleoceanographic data studies based on the analysis of Neodymium (Nd), oxygen and carbon isotopes and sedimentary drift deposits. The oldest record of the NADW initiation dates from the early/middle Eocene boundary (50 - 47 Ma) (Hohbein et al., 2012; Boyle et al., 2017). Borrelli et al. (2014) worked on benthic foraminiferal stable isotope of oxygen and carbon ($\delta^{18}O$ & $\delta^{13}C$), they estimated a thermal offset at $\sim$ 38.5 Ma between the Southern Component Water (SCW) and the North Component Water (NCW) (note that NCW is often referred to as the NADW ancestor). This difference, added to low $\delta^{18}O$ values at this site despite a global cooling trend, suggest that the NADW formation occurred 4 Ma before the Eocene-Oligocene boundary. Miller and Tucholke (1983) suggested that deep water formation in the North Atlantic started during the transition between the Eocene and the Oligocene ($\sim$ 34 Ma) as a consequence of the global cooling and the Antarctic Ice-Sheet (AIS) initiation. Miocene/Pliocene data-based works suggest that NADW formation was already active and highlight a variation of its intensity to reach modern-like intensity (Haug et al., 2001; Kirillova et al., 2019;

Knies et al., 2014). Kirillova et al. (2019) used radiogenic Neodymium records from the Caribbean to suggest that the NADW formation varied from strong to weak modes prior to 9 Ma and then stabilized with the gradual closure of the Central American Seaway (CAS). Another gateway has been proposed to be a key driver of the NADW. The opening of the Fram Strait allowed deep-water mass to exchanges between the Arctic and the Atlantic Ocean and contributed to enhance the NADW formation as suggested by Knies et al. (2014). The contrasted results from these previous studies highlight that the timing of the AMOC onset remains uncertain as do the mechanisms responsible for its triggering.

The closing and opening of ocean gateways influence Earth climate through the ocean circulation that determines the distribution of the ocean conditions. Between the middle Eocene and early Miocene, the configuration of numerous gateways with significant climatic implications underwent substantial changes (Ferreira et al., 2018; Straume et al., 2020) (Figure S1). Starting from the North, the Fram Strait opened at $\sim$ 35 Ma. The connection between the Nordic seas and the North Atlantic deepened over time with the subduction of the Greenland-Scotland Ridge (GSR) (Straume et al., 2020). These Nordic Ocean seaways appear to be critical for the formation of NADW. For instance, Hutchinson et al. (2019) used numerical simulations to show that during the Eocene-Oligocene Transition (EOT; 34 Ma), a closed Fram Strait favours deep convection in the North Atlantic by prohibiting the export of fresh and cold water from the Arctic to the Atlantic. In the more recent context of the Miocene, when Fram Strait was opened, the depth of the GSR was shown to control the northward advection of salt water from subtropical latitudes into the northern seas and to trigger deep convection in the North Atlantic (Vahlenkamp et al., 2018b; Stärz et al., 2017). Further East, the Polish seaway may have played a significant role by connecting the Paratethys to the North Sea as indicated by the upper Eocene pelagic deposits of the Polish Lowlands (Rasser & Harzhauser, 2008; Palcu & Krijgsman, 2021) and microfossil assemblages (Deprez et al., 2015). This seaway became shallower during the Oligocene and closed during the early Miocene (Rasser & Harzhauser, 2008). The closure of the Polish seaway may have led to the cessation of the NADW formation and favoured the initiation of deep water formation in the North Pacific (C. Zhu, Zhang, et al., 2023), by redirecting Arctic waters that initially flowed into the Paratethys towards the North Atlantic. Closer to the Equator, the CAS began to shrink during the middle Eocene (Jaramillo, 2018). The gradual closure of the CAS appears to be a key parameter to initiate the deep water formation in the Atlantic Ocean by precluding freshwater coming from the Pacific to freshen the Atlantic Basin (Sepulchre et al., 2014; Yang et al., 2014). In the Southern Hemisphere, the progressive widening of the Southern Ocean through the opening of the Tasman Gateway between 35.5 and 30.2 Ma (Stickley et al., 2004) and of the Drake Passage between 34 and 30 Ma (Livermore et al., 2005), associated with the initiation of the AIS and global cooling, constitute a tipping point for global ocean dynamics and climate, characterized by the onset of a proto-ACC (Sarkar et al., 2019; Toumoulin et al., 2020).

The global temperature cooled significantly during the Cenozoic era (starting 66 Ma ago; see Hönisch et al. (2023) for a review), which had an impact on the ocean temperature and the stratification. Zhang et al. (2022) made a comparison between eight Global Climate Models (GCM) using early Eocene boundary conditions, and found that the GMOC is relatively insensitive to an increase of atmospheric CO_2 concentrations from 1X to 4X Present Atmospheric Level (PAL).

Here we simulate the climate system for the middle Eocene and the early Miocene using the IPSL CM5A2 model. After validating our simulations through a model-data comparison of sea surface temperature, we conduct a global salt budget analysis to investigate the mechanisms favouring the formation of NADW.

2 Methods

2.1 Model

The Earth system model used in this study is the IPSL-CM5A2 (Sepulchre et al., 2020), based on the Institut Pierre Simon Laplace model for the fifth phase of the Coupled Model Intercomparison Project (CMIP5). It is composed of the atmospheric model from the Laboratoire de Météorologie Dynamique (LMDZ) coupled with a land surface and vegetation model called ORCHIDEE (Krinner et al., 2005), along with an aerosol and chemistry model known as INCA/REPROBUS (Hauglustaine et al., 2004). The ocean component employs the NEMO model (Madec et al., 2016), consisting of three distinct modules: the ocean general circulation model OPA8.2 (Madec et al., 2016), the sea-ice model LIM2 (Fichefet & Maqueda, 1997), and the ocean biochemical model PISCES-v2 (Aumont et al., 2015). The atmospheric regular grid is configured with a resolution of 96 x 96 cells on the horizontal plane and 39 vertical layers. The corresponding horizontal resolution is 3.750° in longitude and 1.875° in latitude. The ocean domain is constituted of a tripolar curvilinear grid of 182 x 149 cells and 31 vertical layers. The longitudinal resolution is 2°, the latitudinal resolution ranging from 0.5° near the Equator to 2° at higher latitudes. Vertical cell thickness varies from 10 m near the surface to 500 m in deeper ocean layers. OASIS (Valcke, 2013) is the coupler used to connect the atmospheric and the oceanic models. The XIOS library manages Input/Output operations. The output comprises climatological data averaged over the last 100 years of the simulations, after 4000 and 3000 years for the Eocene and Miocene simulations respectively, when the deep ocean circulation and temperature have reached an equilibrium.

The results of Sepulchre et al. (2020) show that the modelled Pre-Industrial AMOC reaches an intensity of 10-12 Sv, which is weaker than the AMOC strength observed at 26.5°N reaching 17.2 Sv (McCarthy et al., 2015). The model locations where deep convection occurs are coherent with observations showing deep mixed layer depths in the Greenland Sea. However, in contrast to observations, the control simulation also exhibits deep mixed layers South of Iceland (Sepulchre et al., 2020).

2.2 Simulation Parameters

Two geological periods are investigated in this study: the middle Eocene ($\sim$ 40 Ma) and the early Miocene ($\sim$ 20 Ma). The reconstructions of paleogeography and paleobathymetry for simulating these epochs come from Poblete et al. (2021). The differences in terms of bathymetries and ocean gateways are shown in Figure S1. The main changes between the Eocene and Miocene paleogeographies are the shrinkage of the CAS and Gibraltar and the closure of the Polish strait, while the Southern Ocean gateways (Drake and Tasman passages) are open and deeper during the Miocene.

Here, we reanalyse Eocene and Miocene simulations originally described in Toumoulin et al. (2022) and Pillot et al. (2022) from a different perspective. While Toumoulin et al. (2022) focused on the evolution of continental temperature seasonality and Pillot et al. (2022) investigated the ocean dynamics response to the closure of the eastern Tethys Seaway and the initiation of the Greenland ice sheet, our study focusses on the mechanisms promoting deep water formation in the North Atlantic Ocean, and we aim to gain insights on these processes by comparing Eocene and Miocene simulations performed with the same model. We consider two Eocene simulations. The first one, labelled 40Ma_4X (Table 1), is run with an atmospheric CO_2 concentration equivalent to four times the pre-industrial levels (4X, 1120 ppmv), which is the averaged value during the middle Eocene (Hönisch et al., 2023; Anagnostou et al., 2016; Doria et al., 2011). The second one, labelled 40Ma_2X_ICE, uses an atmospheric CO_2 concentration of 560 ppmv and includes an AIS. Its analysis aims at understanding the impacts of varying atmospheric CO_2 concentration and the presence of an AIS on both climate and ocean circulation dynamics. These Eocene simulations are compared to the Miocene simulation (labelled 20Ma) that includes an AIS and uses an atmospheric CO_2 concentration of 560 ppmv (2X) (Hönisch et al., 2023; Sosdian et al., 2018).

Table 1. Parameters of the simulations for the Eocene (40 Ma) and the Miocene (20 Ma). AIS refers to 'Antarctic Ice Sheet'. The Atlantic Meridional Overturning Circulation (AMOC) corresponds to the maximum of the annual-mean integrated streamfunction at 40°N, deeper than 600 m and the Antarctic Bottom Water (AABW) corresponds to the maximum of the annual-mean integrated streamfunction at 40°S deeper than 200 m, both are expressed in Sverdrup (10^6 m^3/s).

Period	Simulation name	pCO_2 [ppmv]	AIS	AMOC [Sv]	AABW [Sv]
Miocene	20Ma	560	Yes	5	8
Eocene	40Ma_2X_ICE	560	Yes	/	25
Eocene	40Ma_4X	1120	No	/	17

2.3 Model Evaluation

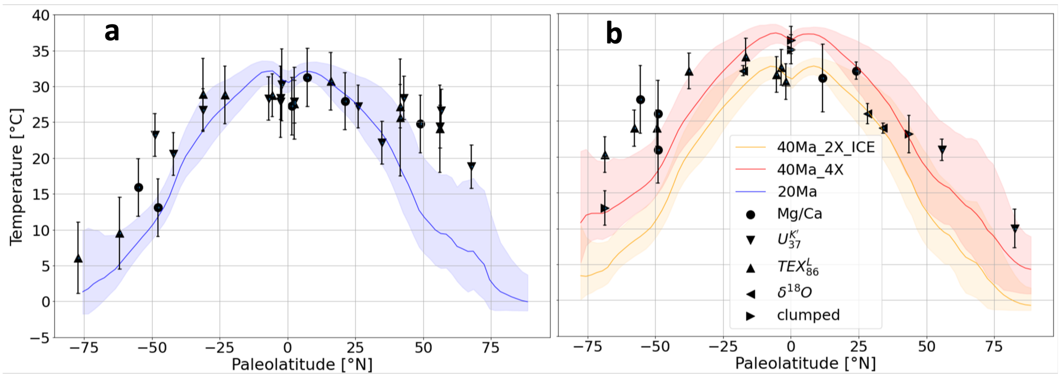

Figure 1. Meridional Sea Surface Temperature (SST) from models, annual-mean values are bold lines, envelopes are bounded with the coolest and the hottest annual-mean values across the 100 years of simulation for each latitude. For the early-middle Miocene (a), SST values are in blue and the SST reconstructed with proxies come from Burls et al. (2021). For the middle-late Eocene (b), SST values are in red (resp. orange) for 40Ma_4X (resp. 40Ma_2X_ICE) and data are from Baatsen et al. (2020).

We first evaluate our different simulations against available proxy reconstructions of sea surface temperatures (SST) for the two epochs. Overall, the global latitudinal variations of SST in our simulations are in good agreement with proxy data from Burls et al. (2021) for the early-mid Miocene (Figure 1a). Temperatures inferred from proxy data and simulated in the model align well in tropical and subtropical regions. However, proxy data infer lower temperatures in the equatorial region and higher temperatures in the northern high latitudes. The Northern Hemisphere meridional temperature gradient is therefore steeper in the model than in the proxy data (Figure 1a). For the late middle Eocene, proxy data from Baatsen et al. (2020) show moderate agreement with the simulated SST (Figure 1b). SST from the 40Ma_4X simulation match the proxy data best, with most of the proxy-inferred SST within the seasonal amplitude. However, the model tends to be warmer than the proxies at low latitudes and colder at high latitudes (Figure 1b). Under a lower atmospheric CO_2 concentration of 560 ppmv and the presence of an AIS, global SST decrease, thereby reducing the model-data bias at low latitudes and increasing it at high latitudes (Figure 1b). Despite these limitations, which are common in model simulations of past warm periods (Burls et al., 2021; Huber, 2012; Lunt et al., 2021), these simulations offer reliable approximations of middle Eocene and early Miocene climatic conditions and render them suitable for our investigation.

3 Results

3.1 Meridional Overturning Circulation and Deep Water Formation

The Miocene fosters the development of ocean deep convection in the North Atlantic, specifically between Greenland and Scotland. This phenomenon is driven by a combination of factors, including surface cooling during winter, sea ice formation and brine release, and increased wind stress, which collectively promote vertical mixing and homogenization of the water column. Here, we use the Mixed Layer Depth (MLD) as a proxy for deep water formation because it highlights the depth at which the ocean surface layer is homogeneous and well-mixed. The MLD in the North Atlantic reaches approximately 1,500 meters (Figure 2) in our Miocene simulation, suggesting the formation of NADW. Sea ice covers the Labrador Sea and the western Norwegian-Greenland Sea during winter (Figure 2). The region where the MLD is maximum is located over the Greenland-Scotland Ridge (GSR). The meridional circulation pattern gives rise to a proto-AMOC with a maximum intensity of $\sim$ 5 Sv (Figure 2, Table 1). Additionally, the GMOC is composed of a counter-clockwise cell originating in the Southern Ocean. There, the mixed layer extends to greater depths, around $\sim$ 4000 meters, generating Antarctic Bottom Water (AABW) with an intensity of 8 Sv (Figure 2, Table 1). Winter MLDs in the 40Ma_2X_ICE Eocene simulation remain shallow ($\sim$ 500 m) in the North Atlantic and this is accompanied by a reduced southern extension of the sea-ice front compared to the 20Ma simulation (Figure 2). In the 40Ma_4X simulation, North Atlantic winter MLDs are even shallower ($\sim$ 250 m), there is no sea ice in winter (Figure2). In the two Eocene simulations, the GMOC is dominated by the Southern Ocean with a strong counter-clockwise cell spanning depths of 500 to 4000 meters and reaching intensities of 25 and 17 Sv for 40Ma_2X_ICE and 40Ma_4X respectively (Figure2, Table 1). In the following, we examine the sea surface property changes between the Eocene and the Miocene that promote the onset of NADW formation in our Miocene simulation (Figure 2).

3.2 Oceanic Surface Properties

The preconditions for deep convection to occur are low vertical density gradients. The properties of deep water are more stable than those of surface water, which is influenced by the wind and the hydrological cycle. Figure S2 shows the horizontal North Atlantic density difference between the 500-meter depth and the surface, highlighting the strength of the vertical density gradient in this region (Figure S2). The Miocene North Atlantic is weakly stratified, particularly in the subpolar and subtropical gyres (Figure S2) with a minimum stratification located in the eastern Norwegian Sea ($\sim$ 1 kg/m^3) and a maximum in the Gulf of Guinea ($\sim$ 9 kg/m^3; Figure S2).

The Brunt-Väisälä frequency (N^2), its thermal (N^2_T) and haline (N^2_S) contributions in the North Atlantic Ocean (Figure S3) depict the vertical density gradient and show that the most buoyant layer is located within the upper 100 meters. The N^2 decomposition allows to decouple the salinity and the temperature effects on the stratification and shows that it is mainly driven by the temperature between 0 - 40°N and by the salinity further North. Meanwhile, the Eocene simulations show stronger stratification overall in the North Atlantic, The thermal and the haline components in the tropical latitudes are stronger at 40 Ma. Over 42 - 59°N, the haline component is also more intense

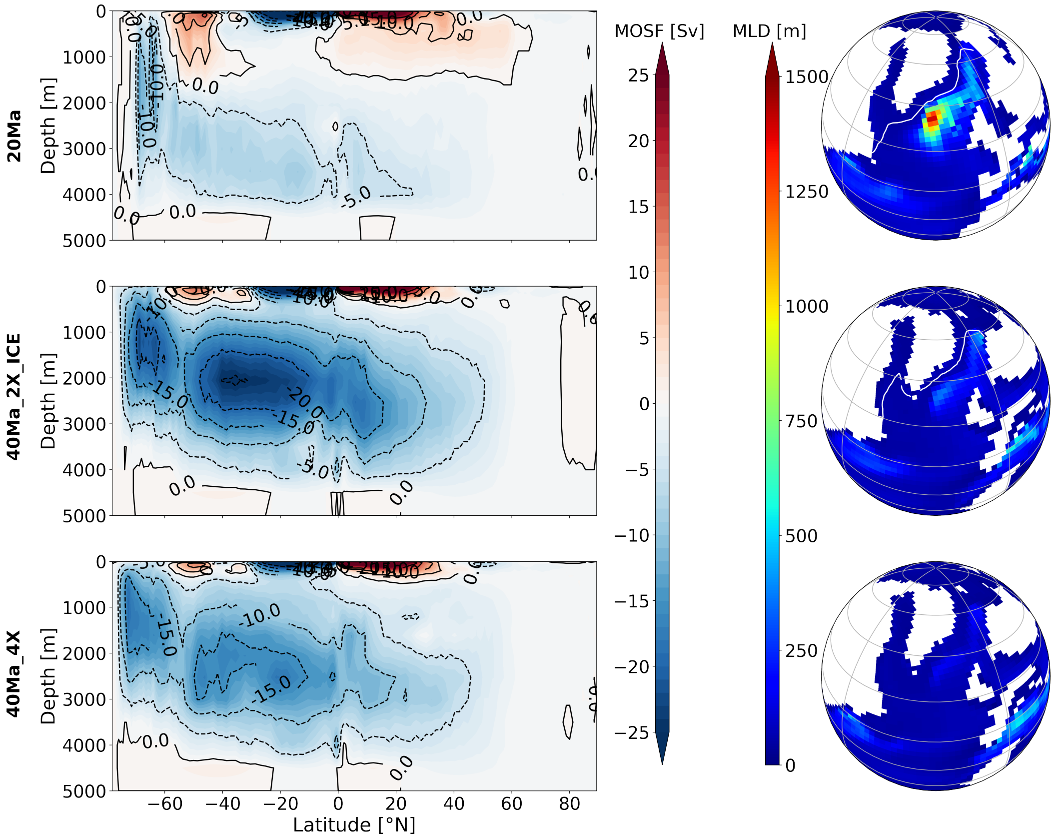

Figure 2. Global meridional overturning stream function averaged over the last 100 years (left), the maximum of the mixed layer depth during the northern Hemisphere winter (from January to March; right) for the 20Ma (top), 40Ma_2X_ICE (middle) and the 40Ma_4X (bottom) simulations. The white lines represent the limit of 10 % of the winter-mean sea ice area fraction.

at 40 Ma (Figure S3). This latitude range corresponds to the Miocene deep convection area.

We thus conclude that the evolution of stratification is mainly due to changes in sea surface properties and that over the latitudes where convection occurs in the North Atlantic Ocean, the stratification is driven by salinity for our three simulations (Figure S3). We will therefore concentrate in the following on water mass property changes in the upper layer (0-100 m).

To understand the causes of these stratification changes between the Miocene and the Eocene, we examine North Atlantic sea density anomaly (density - 1000 kg/m^3, to make the visualisation easier), temperature and salinity in the upper 100 m. During the Miocene the density anomaly is 23.5 kg/m^3 while during the Eocene the upper 100 m layer is globally less dense, with average values of 20.9 kg/m^3 for 40Ma_4X simulation. The largest differences are found in the Greenland Sea and in the Gulf of Guinea, and are particularly pronounced in the 40Ma_4X simulation (Figures 3c, f, i).

The North Atlantic mean SST during the Eocene (40Ma_4X) is 29.1°C with 1120 ppmv, which is 5.8°C warmer than the Miocene. Maximum temperature anomalies are located over the South of the Labrador Sea and through the Central American Seaway (CAS; Figure 3a, g). The temperature differences are weaker between the 40Ma_2X_ICE

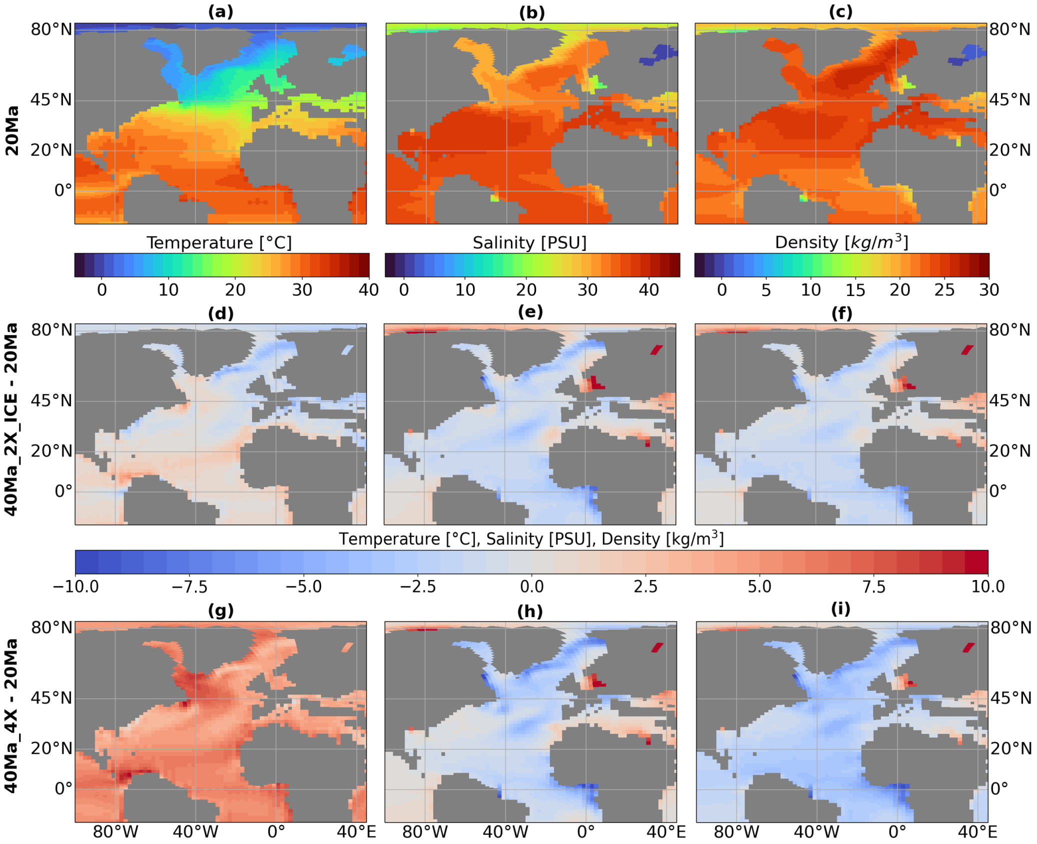

Figure 3. Sea surface temperature (a, d, g), salinity (b, e, h) and density anomaly (density - 1000 kg/m^3) (c, f, i) for the 20Ma (a - c) and the anomalies between 40Ma_2X_ICE and 20Ma (d - f), and 40Ma_4X and 20Ma (g - i).

and 20Ma simulations. Positive temperature anomalies (Eocene warmer than Miocene) are located in the tropical region and in the southern part of the Labrador Sea, contrasting with negative anomalies (Eocene colder than Miocene) along western Europe and most notably in the Norwegian and Greenland seas (Figure 3g).

Furthermore, differences in Sea Surface Salinity (SSS) averaged over the North Atlantic between the Eocene and Miocene epochs, reflect an increase from 34.1 psu for the 40Ma_4X simulation to 35.3 psu for the 20Ma simulation, with maximum negative anomalies concentrated in the western part of the Greenland Sea, between 20-45°N and 20-40°W and over the Gulf of Guinea (Figures 3b, e, h). These differences are again weaker when comparing 40Ma_2X_ICE to 20Ma.

The weaker vertical density gradient in the Miocene is explained by a surface salinity increase that make the upper ocean denser, whereas temperature changes work against an increase in density. In the following sections we investigate oceanic and atmospheric mechanisms that could explain the increase in salinity in the North Atlantic basin in the early Miocene relative to the middle Eocene.

3.3 Oceanic Contribution

We analyze the fluxes across the five straits connected to the North Atlantic: the Fram strait, the Polish Strait, the Central American Seaway (CAS) the Gibraltar strait and Equatorial South America - Africa passage (Figure 4 & 5). In addition to fluxes through these straits, the mean salinity from the surface to 100 m and from 100 to 500 m depth is also computed to determine if the flux brings fresher or saltier water within the Atlantic. These two depth ranges correspond approximately to the transport reversal through the Fram strait and the CAS (Figures 5 g, i).

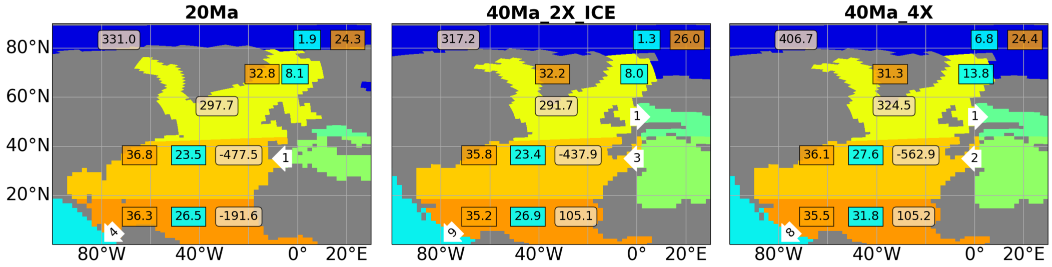

Figure 4. The North Atlantic basin is divided in three sub-basins by latitudes, the tropics (dark orange), sub-tropics (orange) and the polar (yellow); the Arctic (blue), the Pacific (light blue) Ocean and the Tethys Sea (green) basin are also represented. In each box the surface freshwater flux is calculated (Precipitation - Evaporation + Runoff + Sea ice melting) and indicated in the light orange boxes (mSv), the mean salinity (orange) and temperature (blue) for each basin is averaged over the first 100 meters and are expressed in PSU and °C respectively. The fluxes, integrated over the upper 100 m, between the basins are represented with the white arrows (Sv).

The connection between the Arctic and the Atlantic becomes narrower and deeper from the Eocene to the Miocene (Figure 5a-c, g). In all of the simulations, the Arctic Ocean exports fresh water in the deep water formation area via the Fram Strait, mostly within the upper 100 m. The transport across the top 100 m of the strait is 1.4 Sv in 20Ma, which is weaker by 0.2 and 0.1 Sv in comparison to 40Ma_2X_ICE and 40Ma_4X respectively (Figure 5a-c, g). Deeper, the direction of transport reverses, going from the Norwegian-Greenland Sea to the Arctic. This northward flux is 1.1 Sv for 20Ma, 1.3 Sv for 40Ma_2X_ICE and 1.2 Sv for 40Ma_4X (Figure 5d-g). The depth range over which this northward flux occurs is between 300-600 m at 20 Ma and between 100-400 m at 40 Ma.

In the equatorial band, the Gibraltar Strait makes the connection between the Mediterranean Tethys and the subtropical North Atlantic basin. The Mediterranean Tethys is an evaporative basin, contributing to the formation of salty surface water, particularly evident in the 40Ma_4X simulation (Figure 5a-c). The shrinkage of the Tethys Sea, the gradual closure of the Eastern Tethys Seaway, and the narrowing of the Gibraltar Strait occurred between the Eocene and the Miocene, and collectively result in a weak surface transport through Gibraltar Strait during the Miocene (-1 Sv; Figure 4 & Figures 5c, j), leading to a small input of salt from the Mediterranean Tethys to the Atlantic (Figure 4). The westward transport through Gibraltar in the upper 100 m is larger in 40Ma_2X_ICE and 40Ma_4X, reaching as high as -3 Sv, and thus carries more salt into the tropical Atlantic. The westward transport is also more intense below 200 m depth for all the simulations, with a total flux of -4.7 Sv for 20Ma, -14.2 Sv for 40Ma_2X_ICE and -12.6 Sv for 40Ma_4X (Figures 5c, f, j).

South tropical waters are advected along the North Brazilian coasts northwestward along with the South Equatorial current in the upper 100 m. The total flux across the Equator is 4.0 Sv for 20Ma and is stronger at the Eocene, reaching 5.8 and 6.1 Sv for 40Ma_2X_ICE and 40Ma_4X (Figures 5a - c, k - m). On the eastern side of the equatorial Atlantic, the surface waters flow southward with a cumulative flux of -2.8, -3.6 and -3.9 Sv for 20Ma, 40Ma_2X_ICE and 40Ma_4X respectively.

The surface leakage to the Pacific Ocean through the CAS is 4 Sv for 20Ma, while in the Eocene simulations the transports are twice as strong and reach 9 and 8 Sv for 40Ma_2X_ICE and 40Ma_4X respectively (Figure 4 & Figures 5a-c, j). This salt outflow is primarily driven by the horizontal ocean circulation, featuring a strong (15 Sv) cyclonic gyre that transports water westward from the Mediterranean Tethys Sea to the Pacific Ocean (Figure 6b-c) during the Eocene. This Miocene reduction in surface leakage reduces the export of salt originating from the Mediterranean Tethys Sea and from the South Atlantic to the Pacific Ocean and thus contributes to the salinification of the surface layer in the tropical and subtropical Atlantic basins during the Miocene (Figure 4 & Figures 5a-c, i-m). The upper 100 m outgoing flux from the Atlantic across the CAS in Eocene simulations (9 and 8 Sv for 40Ma_2X_ICE and 40Ma_4X resp., Figure 4) is equal to the sum of the ingoing flux from the Mediterranean Tethys via Gibraltar (3 and 2 Sv for 40Ma_2X_ICE and 40Ma_4X resp., Figure 4) and the ingoing flux from the South equatorial Atlantic (5.8 and 6.1 Sv for 40Ma_2X_ICE and 40Ma_4X resp., Figure 5l-m) while 1 Sv recirculate in the North Atlantic for 20Ma with 4 Sv out-flowing via the CAS and 1 and 4 Sv inflowing via Gibraltar and the Equator respectively (Figures 5k & 4). The average salinity over the top 100 meters reaches 36.3 and 36.8 psu in the Tropical and subtropical Atlantic basins respectively during the Miocene. In comparison, these values are 35.2 and 35.8 psu for the 40Ma_2X_ICE simulation, and 35.5 and 36.1 psu for the 40Ma_4X simulation (Figure 4).

These changes in water transport through the straits encircling the North Atlantic Ocean are evidently influenced by the global ocean circulation and, in particular, the gyre circulation that also changed significantly between the two periods (Figure 6a-c).

Under Miocene paleogeographic conditions, the subpolar cyclonic gyre extends northeast into the Norwegian Sea, with the 5 Sv contour encompassing the region 45-2°W and 41-70°N. Notably, the maximum of the barotropic stream-function reaches 21 Sv, and its location corresponds with the deep convection area (Figure 2 & 6a-c). In the 40Ma_4X simulation, the gyre is restricted within the region bounded by 21-35°W and 50-58°N, delineated by the 5 Sv contour (Figure 6c). The gyre is weak ($\sim$ 6 Sv). When halving the atmospheric CO_2 concentration (40Ma_2X_ICE), the subpolar gyre expands towards the Labrador Sea, spanning an area between 18-42°W and 42-59°N, and intensifies to around 9 Sv (Figure 6b). The widening of the North Atlantic basin due to the northward displacement of Greenland and the deepening of the Atlantic Ocean contributes to the expansion of the subpolar gyre during the Miocene. An other driver may have been changes of the mean atmospheric circulation. Over the subpolar gyre, the wind stress curl is positive in all the simulations, inducing a cyclonic circulation and upwells sub-surface water through Ekman pumping. Yet,this positive signal is bounded in the Norwegian-Greenland Sea to 62°N for the Eocene simulations while it reaches 70°N for the Miocene simulation (Figures 6a, d-f). In our simulations, the dynamics of the subpolar gyre is also affected by the closure of the Polish Strait (connecting the North Sea to the Para-Tethys Sea) that occurred between the Eocene and the Miocene (Palcu & Krijgsman, 2021). About 1 Sv of water is indeed exported across the top 100 m from the subpolar gyre to the Para-Tethys Sea under Eocene paleogeographic conditions(Figures 5h & 4), thereby impacting the strength and northern extension of the gyre (Figures 6).

The subtropical gyre also plays a crucial role in transporting salt and heat from the Gulf of Mexico to western Europe via an eastern boundary current similar to the modern Gulf Stream. Its intensity varies between simulations, with values of $\sim$ 23 Sv for 20Ma, $\sim$ 20 Sv for 40Ma_2X_ICE and $\sim$ 15 Sv for the 40Ma_4X (Figures 6a-c). These changes in gyre intensity and shape result in the northward advection of saltier and warmer water from the subtropical to subpolar gyre during the Miocene, resulting in salinity and

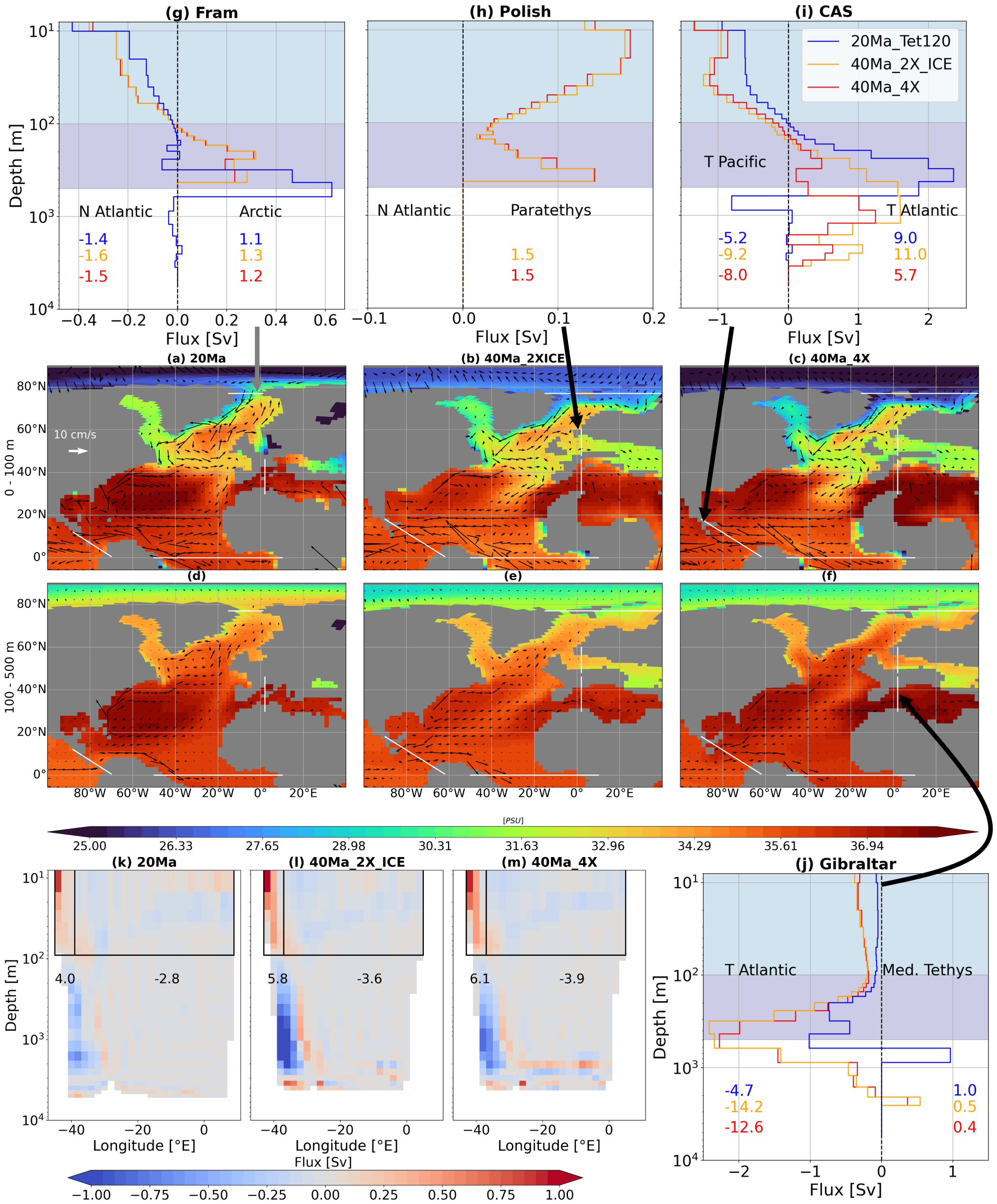

Figure 5. Annual-mean salinity and horizontal velocity (arrows) averaged between the surface and 100 m (a-c) and between 100 and 500 m (d-f). The white strait lines represent the straits and the transport per depth (in Sv) across these straits are represented (g-j). The transports for 20Ma, 40Ma_2X_ICE and 40Ma_4X are represented with the red, orange and blue lines respectively, and the integrated transports (their positive and negative contributions) are indicated at the bottom in the same colours. Note that a positive value indicates a transport to the north and to the east. In (g-j), the light and dark blue shadings represent the averaged depth range used for the salinity maps in (a-f). Vertical meridional flux through the equatorial South America-Africa passage (k-m) for 20Ma (k), 40Ma_2X_ICE (l) and 40Ma_4X (m), with the integrated transport in the respective boxes indicated below them.

sea surface density anomalies between Eocene and Miocene simulations in the subtropics (Figures 3e, f, h, i).

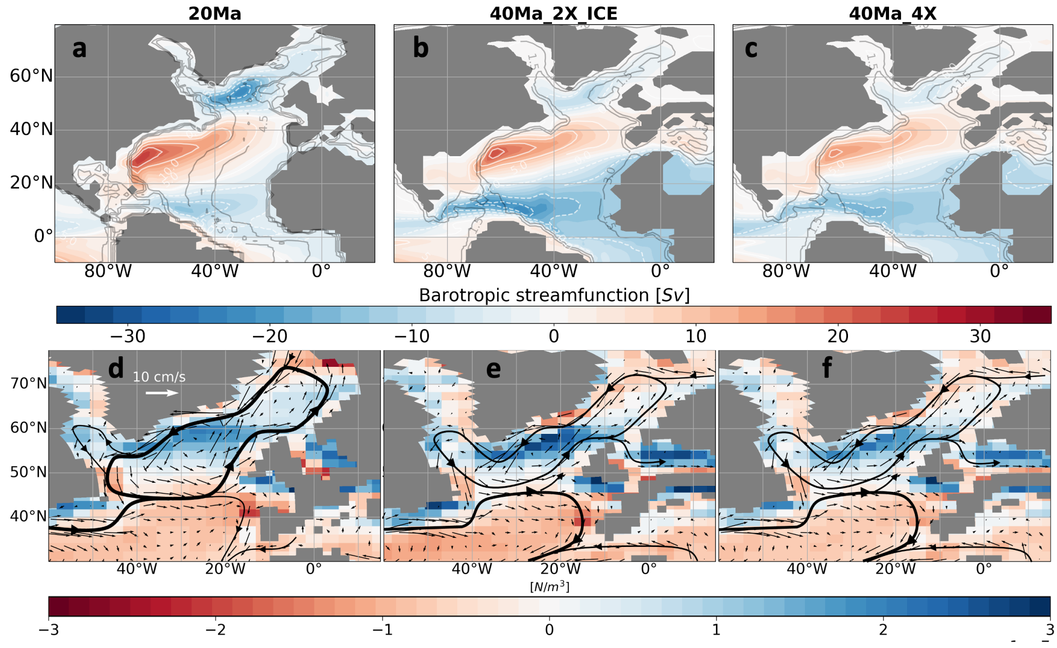

Figure 6. Barotropic streamfunction (in Sv) of the North Atlantic for the 20Ma (a), 40Ma_2X_ICE (b) and 40Ma_4X (c) simulations. The fields are averaged over 100 years. The white (black) lines correspond to the isolines of the barotropic streamfunction (bathymetry), increasing by 5 Sv (1.5 km). Wind stress curl (in N/m^3) and currents (in cm/s) averaged over the top 100 m over the North Atlantic basin for the 20Ma (e), 40Ma_2X_ICE (f) and 40Ma_4X (g) simulations. The main gyres are drawn on top with black lines, their relative width indicating the intensity.

Table 2. Meridional transport (in Sv) within the upper 100 m across 45°N in the Atlantic Ocean, decomposed in their northward, southward and the net components for the 40Ma_4X, the 40Ma_2X_ICE and the 20Ma simulations.

Period	Simulation	Northern flux [Sv]	Southern flux [Sv]	Net flux [Sv]
Miocene	20Ma	1.00	-1.79	-0.79
Eocene	40Ma_2X_ICE	0.58	-2.15	-1.57
Eocene	40Ma_4X	0.34	-2.28	-1.94

Finally, there is a need to consider the connections between the subtropical and subpolar gyres. Overall, there is a net southward transport over the top 100 m across 45°N, with varying magnitudes in the different simulations -0.79 Sv for 20Ma, -1.57 Sv for 40Ma_2X_ICE and -1.94 Sv for 40Ma_4X (Table 2). The northward fluxes are 1 Sv for 20Ma and decreases to 0.58 and 0.34 Sv for 40Ma_2X_ICE and 40Ma_4X respectively. While the intensity of the subtropical gyre for 20Ma and 40Ma_2X_ICE are close, their shape are different. The western boundary current mainly advects water towards lower latitudes at

40 Ma, with a weak salt transport towards the subpolar gyre. Whereas during the Miocene, this transport is significant and contributes to the salinification of the subpolar gyre.

3.4 Atmospheric Contribution

In addition to ocean circulation changes, changes in the atmospheric forcing may have contributed to alter surface layer properties between the Eocene and Miocene, as a result of different large scale atmospheric circulations. To quantify this contribution, we compute a freshwater budget for two regions, the polar North Atlantic and the tropical North Atlantic, considering the different component of the surface freshwater flux (Figure 7a). Note that the same budget for the subtropical North Atlantic is shown in Figure S4.

The net surface freshwater flux over the polar North Atlantic are 297.7 mSv, 291.7 mSv and 324.5 mSv for the 20Ma, 40Ma_2X_ICE and 40Ma_4X simulations, respectively (Figures 4 & 7). It means that the Miocene polar North Atlantic receives ∼ 10 % less freshwater in comparison to the 40Ma_4X simulation and an equivalent amount as 40MA_2X_ICE (-6 mSv). The contribution from sea-ice processes remains small overall, including in the two simulations in which the sea-ice extent is significant (Figure 2), suggesting that, on average, the integrated contribution of sea ice melting and freezing in the region cancel each other out over the seasonal cycle. The contribution of P-E over the ocean is weaker at 20 Ma. Specifically, P-E averaged over the North Atlantic basin at 20 Ma is 113.5 mSv and increases by 11.9 mSv and 31.5 mSv for the 40Ma_2X_ICE and 40Ma_4X simulations respectively (Figures 4, 7). P-E anomalies along southeastern coasts of Greenland during the Eocene result from the northward displacement of Greenland and variations in Greenland topography affecting 850 hPa isobars (Figure 7e-g). The North Sea receives more freshwater from the atmosphere at 40 Ma (Figures 7b-d) due to the differences in the high pressure cell extending eastward and further South than for 20Ma (Figures 7e-g). The total runoff reaching the PNA basin during the Miocene amounts to 137.0 mSv, which is roughly equal to the value for 40Ma_2X_ICE (Figure 7a) but is much lower than the runoff outflowing in the PNA basin in the 40Ma_4X simulation (difference of 40.3 mSv). This is due to larger precipitations over northeastern North America and Greenland in the 40Ma_4X simulation. Another important parameter influencing the net surface freshwater flux is the area of watersheds outflowing in the North Atlantic, which is significantly smaller over North America in our Miocene simulation compared to the Eocene. Their surfaces are 7.8 10^6 km^2 at 20 Ma but 14.2 10^6 km^2 at 40 Ma (Figure 7b-d). As a result, there is a large runoff from North America with 139 and 133 mSv for 40Ma_4X and 40Ma_2X_ICE and 82 mSv for 20Ma (not shown), that contributes to a fresher Eocene North Atlantic (Figure S5).

The total freshwater flux in the subtropical North Atlantic is negative for the three simulations, because it is an evaporative basin (Figure S4). The net flux are relatively similar in the 20Ma and 40Ma_2X_ICE simulations, amounting to -477.5 and -452.0 mSv, while it amounts to -562.9 mSv in the 40Ma_4X simulation. The differences in runoff contribution are ∼10 mSv between the simulations, indicating that, in this basin, the differences in net freshwater flux are associated to changes in the hydrological cycle over the ocean rather than land. The changes are associated with a modulation of the anticyclonic circulation, as shown by higher pressure at 850 hPa in 40Ma_4X compared to 40Ma_2X_ICE and 20Ma (Figure 7 e-g) that favours an increase in air temperature and evaporation (not shown). The eastern side of the subtropical North Atlantic is more evaporative at 20 Ma (Figures 7b-d). This difference is more marked in the 40Ma_2X_ICE simulation and is due to a weaker zonal atmospheric pressure gradient West of Gibraltar (Figures 7e-g).

In the tropical basin, the net surface freshwater flux is negative in the Miocene simulation but positive in the Eocene simulations, with mean values of -195.6, 105.1, and

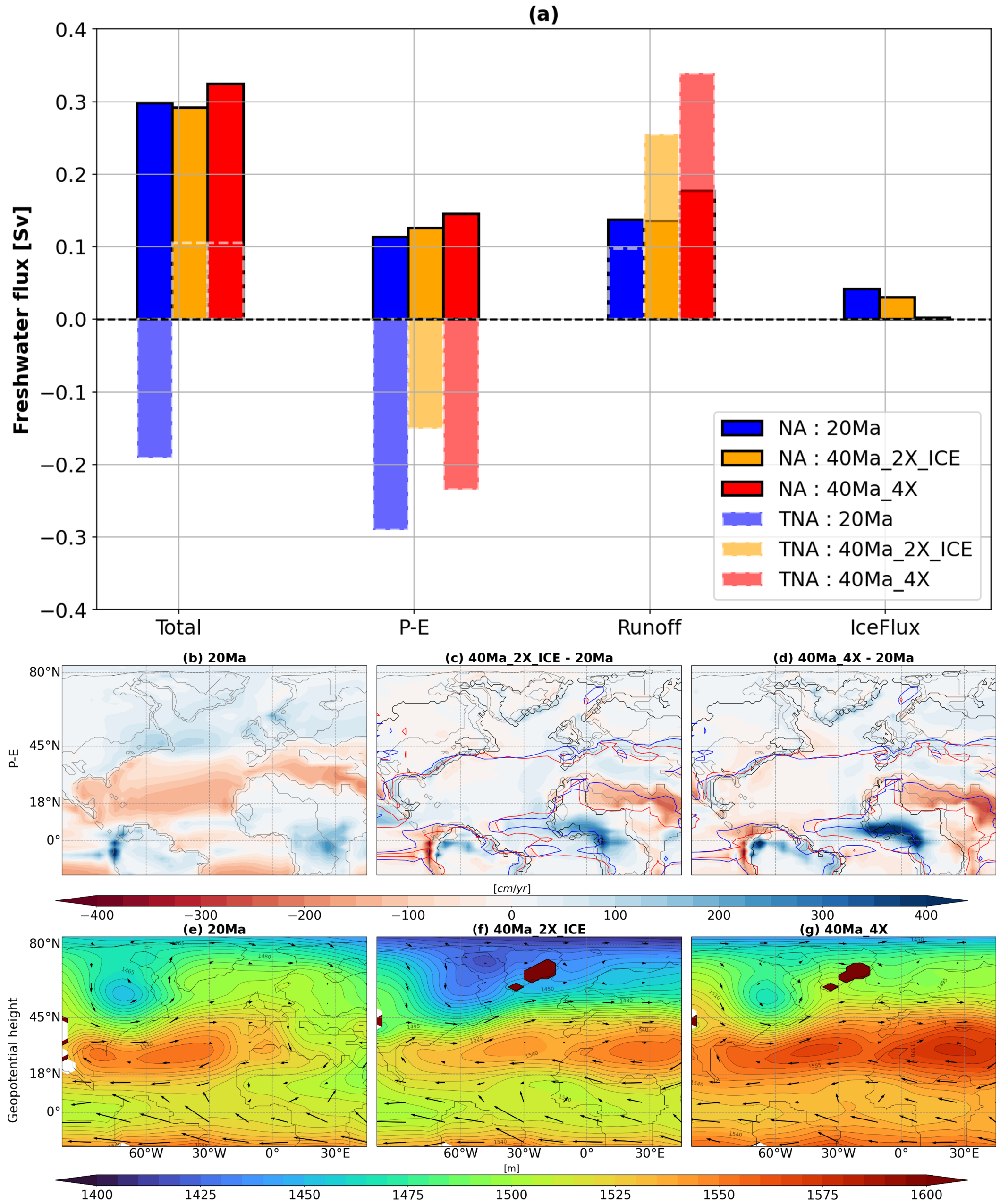

Figure 7. Bar chart (a) representing the total freshwater surface flux over the ocean (Total), and the contributions from the Precipitation minus Evaporation (P-E), the runoff (Runoff) and the freshwater from the sea ice melting and freezing (IceFlux). Bars with with continuous and dashed contours represent the Polar North Atlantic (PNA) and the Tropical North Atlantic (TNA). Maps of mean P-E (b; in cm/yr) and geopotential height (in m; colors) winds (in cm/s; vectors) at 850 hPa (e) and for the 20Ma simulation. Maps of the anomalies (compared to 20Ma) of P-E (c, d) and geopotential height at 850 hPa (f, g) for the 40Ma_2X_ICE (c, f) and 40Ma_4X (d, g) simulations. On the P-E maps, the gray and black lines represent the watersheds connected to the Atlantic Ocean at 20 Ma and 40 Ma, respectively, and 0 contours are drawn in blue and red at 20 Ma and 40 Ma, respectively.

105.2 mSv for the 20Ma, 40Ma_2X_ICE and 40Ma_4X simulations, respectively (Figure 4). Over this band of latitudes, the freshwater budget is dominated by oceanic evaporation, which leads to negative P-E in the three simulations, particularly at 20 Ma (P-E = -290.5 mSv) and slightly less so at 40 Ma (-150.3 and -234.4 mSv in 40Ma_2X_ICE and 40Ma_4X respectively) (Figure 7a). The runoff contribution is small at 20 Ma (97.9 mSv), whereas significant runoff fluxes are found during the Eocene (255.4 and 339.5 mSv for the 40Ma_2X_ICE and 40Ma_4X simulations; Figure 7 a). This is primarily explained by a shift in the location of intense precipitation that largely reroutes continental runoff to the Indian Ocean rather than the Atlantic Ocean, and is the result of a change in large-scale atmospheric circulation. In the Eocene, an anticyclonic atmospheric circulation extends zonally from the Gulf of Mexico to India (Figure 7e-g), whereas it is confined to the Atlantic Ocean in the Miocene, because of the different paleogeography of Africa and the associated shrinkage of the Tethys Sea. This circulation change impacts trade winds over Africa and the African monsoon, and relocates the area of maximum precipitation, which coincides with the location of the equatorial lower pressure cell, from western equatorial Africa in the Eocene to eastern equatorial Africa in the Miocene. Precipitations reach approximately 600 cm/yr in 40Ma_4X and slightly decrease to around 500 cm/yr in 40Ma_2X_ICE, due to the halving of the atmospheric CO_2 concentration and the associated reduction in hydrological cycle intensity (Figure 7 b-c). During the Miocene, the precipitation maximum is even weaker (around 400 cm/yr; Figure 7c), which contributes to decreasing the amount of runoff received by the tropical NA basin in the Miocene.

In summary, total freshwater inputs to the North Atlantic and subtropical North Atlantic basins remain consistent across the three simulations: in spite of changes in the magnitude of the fluxes, the North Atlantic gains freshwater whereas the subtropical North Atlantic exports it. In contrast, the tropical North Atlantic shifts from a positive to a negative net freshwater input between the Eocene and the Miocene. This inversion is primarily attributed to a weakening and eastward displacement of African monsoon precipitations, driven by alterations in African trade wind patterns.

4 Discussion

4.1 Timing of the Initiation of the North Atlantic Deep Water Formation

The timing of the proto-North Atlantic Deep Water (NADW) initiation remains a subject of debate. Evidence from contourite drifts in the North Atlantic suggests onset during the early to middle Eocene, marked by increasing terrigenous mass accumulation rates and starting aggradation of contourite drifts (Boyle et al., 2017; Hohbein et al., 2012). However, the benthic foraminiferal records indicate deep convection as early as the late Eocene or the Eocene-Oligocene Transition (EOT) (Borrelli et al., 2014; Coxall et al., 2018; Katz et al., 2011; Miller & Tucholke, 1983). Borrelli et al. (2014) reported thermal gradients at ∼38.5 Ma linked to the differentiation of NADW and the Southern Component Water (SCW), with intensification coinciding with the gradual Southern Ocean opening. Similarly, Parent et al. (2024) observed a Deep Western Boundary Current (DWBC) before ∼35 Ma followed by a progressive strengthening using terrigenous grain size and geochemical data. Coxall et al. (2018) identified a transient NADW pulse between ∼35.8 and ∼33.8 Ma, with a permanent establishment after ∼34.3 Ma based on excursions of $\delta^{13}C$ values in the North Atlantic. Katz et al. (2011) proposed that the NADW onset and the later gradual intensification is related to the strengthening and the deepening of the Antarctic Circumpolar Current (ACC) after ∼31 Ma. During the Oligocene and Miocene, a decline in radiogenic neodymium values in the Southern Ocean is attributed to an increase in the export of NADW (Scher & Martin, 2008). This southward NADW export fluctuated during the middle to late Miocene, reaching modern-like rates after 9 Ma, as indicated by radiogenic neodymium records (Kirillova et al., 2019). The timing and progression of NADW initiation remain debated, with contrasting hypotheses suggesting gradual intensification or episodic pulses and rapid transitions in its development.

Model simulations provide further insight into this debate. Some studies have successfully reproduced a proto-NADW and associated proto-AMOC during the early to middle Eocene under specific conditions (Huber & Sloan, 2001; Huber et al., 2003; Vahlenkamp et al., 2018a, 2018b; C. Zhu, Zhang, et al., 2023). For instance Huber et al. (2003) and Vahlenkamp et al. (2018b) show that restricting the Nordic Straits, thereby limiting Arctic freshwater outflow, facilitates proto-NADW formation. Vahlenkamp et al. (2018a) further demonstrate the sensitivity of NADW formation to orbital parameters, particularly low obliquity conditions. However, results from the Deep-Time Model Intercomparison Project (DeepMIP) (Zhang et al., 2022) highlight the model-dependent nature of proto-AMOC, with only two out of eight models simulating its presence under the same early Eocene paleogeographic conditions.

Focusing on the late Eocene, Hutchinson et al. (2019) and Straume et al. (2022) also find deep water formation in the North Atlantic under conditions where Arctic-North Atlantic connections were closed. Conversely, other models (Baatsen et al., 2020; Goldner et al., 2014) suggest an overturning circulation primarily driven by the Southern Ocean. This overview indicates that deep water formation in the North Atlantic during the Eocene is less commonly simulated than in the Southern Ocean and, when present, is often dependent on restricted Arctic-North Atlantic water exchange.

Our simulations show no NADW formation under middle Eocene boundary conditions but indicate its emergence alongside a proto-AMOC during the early Miocene. These results align with paleoceanographic evidence suggesting a late Eocene to EOT onset of deep water formation in the North Atlantic (Borrelli et al., 2014; Coxall et al., 2018; Katz et al., 2011; Miller & Tucholke, 1983) and are consistent with most DeepMIP models (Zhang et al., 2022). However, they contradict the earlier onset of the Eocene proposed by proxy-based studies (Boyle et al., 2017; Hohbein et al., 2012) and model-based studies (Huber & Sloan, 2001; Huber et al., 2003; Vahlenkamp et al., 2018a, 2018b; C. Zhu, Zhang, et al., 2023) that suggest an earlier onset in the Eocene. As previously noted, Eocene proto-AMOC simulations typically require a closed Arctic-North Atlantic connection. In our study, this connection remains open, allowing Arctic freshwater outflow, which inhibits deep water formation.

Although our comparison of these two time periods does not definitively pinpoint the early Miocene as the NADW initiation time, it does narrow down the potential time frame. To further constrain this window, future studies should incorporate detailed paleogeographic reconstructions of the Oligocene, including changes in gateways and varying atmospheric CO_2 concentration levels. This will allow for a more refined temporal scenario of NADW development.

4.2 Mechanisms Favouring the NADW Formation

4.2.1 Inter-Basin Oceanic Exchanges

The geometry of the Nordic seaways, and in particular the Fram Strait and Greenland-Scotland Ridge (GSR), significantly influences the initiation and location of the NADW. While the Fram Strait began to open in the early Eocene (Engen et al., 2008; Straume et al., 2020), its impact on ocean circulation remains debated. In the Eocene, the studies suggest that the response to the opening of the Fram Strait lead to a weakening or a cessation of the NADW (Hutchinson et al., 2019; Vahlenkamp et al., 2018b; Straume et al., 2022). Those findings are in agreement with our Eocene simulations, demonstrating that an open and deep Fram Strait prevent deep convection in the North Atlantic. On the other hand, in the Miocene, the opening of the Fram Strait strengthens the NADW (Hossain et al., 2020). This result is in line with our early Miocene simulation depicting a proto-AMOC with a wide and deep Fram Strait, suggesting that additional factors control the North Atlantic stratification at that time.

The Polish Strait, which connected the Paratethys to the North Sea, was open during the Eocene but closed during the early Miocene (Palcu & Krijgsman, 2021; Rasser & Harzhauser, 2008). This seaway has most likely a significant impact on global circulation. C. Zhu, Liu, et al. (2023) found that the closure of the Polish Strait during the early Eocene caused the cessation of the AMOC, as fresh and cold Arctic water that would have flowed into the Paratethys were instead trapped in the North Atlantic, enhancing local stratification. This finding contrasts with our results, where we suggest that surface water flowing into the Paratethys via the Polish Strait originated from the North Atlantic, not the Arctic. The result is an export of salt and a weakening of the subpolar gyre intensity, both of which inhibit deep water formation in the North Atlantic. This difference is likely due to the differences with paleogeographies used by C. Zhu, Liu, et al. (2023), which considered a paleogeography of the early Eocene with an open Turgai Strait. Instead, our study is based on a middle Eocene configuration where the Turgai Strait is closed, isolating the Arctic from the Paratethys.

The Atlantic Ocean's salt balance is influenced by the advection of salty water from the tropical South Atlantic and the Mediterranean Tethys Sea, while the transport through the Central American Seaway (CAS) represents a loss of salt. Despite larger salt inputs in the Eocene, the Miocene sea surface remains saltier due to reduced westward wind-driven currents transporting Atlantic water to the Pacific via the CAS at this time. This salt leakage was significantly higher in the Eocene compared to the Miocene (from 9 to 4 Sv). While the closure of the eastern Tethys seaway in the Miocene had little impact on the NADW formation (Pillot et al., 2022), the connection between the Mediterranean Tethys and the Atlantic appears critical. Indeed, Ivanovic et al. (2014) suggest that the cessation of the advection of salty water across this later gateway contributed to a slowdown of the AMOC during the late Miocene.

Regarding the export of salty water, our findings align with previous studies (Kirillova et al., 2019; Nisancioglu et al., 2003; Sepulchre et al., 2014) indicating that the gradual shoaling of the CAS played a crucial role in triggering or enhancing NADW formation by limiting the Atlantic outflow into the Pacific. This low-latitude salinity signal originates far from the deep convection region but is advected to the northern Atlantic Ocean by the large-scale wind-driven gyres.

4.2.2 Gyre Dynamics

The North Atlantic subtropical and subpolar gyres undergo significant expansion between our middle Eocene and early Miocene simulations. This expansion is primarily driven by the widening of the Atlantic Ocean basin and the gradual closure of equatorial seaways. An additional effect is the drawdown of atmospheric CO_2 as shown by our middle Eocene simulations with an increase in intensity from 6 to 9 Sv owing to the steeper meridional surface temperature gradient. Paleogeographic forcings further intensifies the gyres in the early Miocene simulations. Altogether, these processes contribute to form a stronger early Miocene subpolar gyre (21 Sv) compared to the middle Eocene (6-9 Sv). Exchanges between the subtropical and subpolar gyres also intensify with the decrease in atmospheric CO_2 concentration, increasing from 0.34 to 0.58 Sv in our middle Eocene simulations and reaching 1.0 Sv in the early Miocene simulation. This intensification is primarily attributed to the strengthening of the Norwegian Current, which transports saline waters within the subpolar gyre and to the deep convection zone.

These findings align with previous studies by Herold et al. (2012) and Zhang et al. (2020), which compared Miocene and Modern climates, as well as early Eocene and Pre-Industrial climates, respectively. They found that paleogeographic forcings influence gyres intensity through the widening of the Atlantic Ocean and the gradual closure of the equatorial straits. Additionally, Hutchinson et al. (2018) and Zhang et al. (2020) demonstrated that decreased atmospheric CO_2 concentration tend to enhance the gyre circulation intensity, through a steepening of the meridional surface temperature gradient, a phenomenon known as 'polar amplification' (Alexeev et al., 2005). Moreover, the intensification of the cyclonic subpolar gyre uplifts isopycnals due Ekman pumping, and thus promotes the occurrence of deep convection (Fedorov et al., 2023; Marshall & Schott, 1999). As such, the enhanced northward salt transport from the subtropical to the subpolar gyre in the early Miocene favoured the formation of NADW (Ferreira et al., 2018).

4.2.3 Hydrological cycle

The hydrological cycle significantly impacts sea surface density and stratification. A key difference between the Eocene and Miocene simulations is found at the tropical latitudes. The African monsoon regime transitioned from intense precipitations over the west-central Africa and the Gulf of Guinea in the Eocene, to weaker and more localized precipitations over central Africa in the Miocene. This change results from a decrease in freshwater flow in the tropical North Atlantic, from 105 mSv during the middle Eocene to -192 mSv during the early Miocene, coupled with an increase in salinity from 35.5 psu to 36.3 psu (Figure 4), reflecting the impact of freshwater flux changes on the salinity variation within the region. This shift is attributed to the contraction of the anticyclonic atmospheric circulation in the subtropics during the Miocene, resulting from the Tethys Sea's shrinkage and the relocation of the equatorial low-pressure band over central Africa. A significant portion of Miocene precipitations therefore occurs over the Indian Ocean watershed, thus reducing runoff input to the Atlantic Ocean. Additionally, halving the atmospheric CO_2 concentration in the Eocene leads to a reduction in the amount of precipitations induced by the African monsoon in our simulations. These findings align with previous studies (Fluteau et al., 1999; Acosta et al., 2022) that suggested a weakening of the African monsoon over time due to the Tethys Sea's shrinkage and the northward drift of Africa. Acosta et al. (2022) specifically found a weakening of the West African monsoon between the early Eocene and middle Miocene, linked to the widening of the South Atlantic basin and reduced moisture advection from South America. They also found a strengthening of the monsoon when rising atmospheric CO_2 concentration in the Miocene, although the precipitation spatial pattern remained unchanged. The resulting salinification of the Atlantic at low latitudes during the Miocene is then advected towards the high latitudes (Section 4.2.2), further contributing to weakening the stratification and favouring the formation of NADW. Though our results point towards a direct role for the displacement and weakening of the African monsoon in the salinification of the tropical Atlantic and subsequent advection of this salt into the North Atlantic, the extent to which this process contributes to the effective onset of the NADW should be further explored using dedicated freshwater hosing experiments.

4.2.4 Climate Forcing

Our simulations demonstrate that the simulated middle Eocene climate is sensitive to reductions in atmospheric CO_2 concentrations and the initiation of the AIS, that induce a global cooling accompanied by a strengthening of the ocean and atmospheric dynamics, including stronger trade winds, westerlies, and ocean gyres. This intensification is driven by the steepening of the meridional surface temperature gradient (Hutchinson et al., 2018; Zhang et al., 2020). Concurrently, the freshwater surface flux into the Atlantic Ocean decreases (Figure 4 & 7 ; Acosta et al. (2022)).

While these changes create favourable conditions for NADW formation, the Eocene paleogeography ultimately prevents it. This finding aligns with sensitivity tests described in Zhang et al. (2020), which revealed minimal changes in ocean circulation with varying atmospheric CO_2 concentrations. Conversely, the Miocene paleogeography facilitates

NADW formation, and its intensity appears to be influenced by climatic forcings (Crichton et al., 2021).

It can be inferred that both paleogeographic and climatic factors played significant roles in the initiation of NADW. However, paleogeography appears to have been the primary driver, with cooling likely serving as a necessary prerequisite for NADW formation or a modulation of its formation's rate, as suggested by Vahlenkamp et al. (2018a).

4.3 Limitations and Perspectives

Our study contributes to the growing body of literature on the Cenozoic history of the NADW/AMOC, with a focus on identifying the physical processes driving deep convection in the North Atlantic Ocean from the middle Eocene to early Miocene. Paleogeography and ocean gateways play a critical role in ocean circulation. However, significant uncertainties remain regarding their configurations and the timing of their evolution. The boundary conditions influence the simulation outcomes. In this study, we employ the paleogeographic reconstructions of Poblete et al. (2021), which represent a significant advancement for the community by providing consistent paleogeographies spanning the entire Cenozoic. However, it is uncertain whether our results would be consistent with other reconstructions without conducting an ensemble of simulations using different paleogeographies, conducting sensitivity tests with key gateways, ice-sheet and at different atmospheric CO_2 concentrations. Additionally, the location of runoff discharge into the ocean could affect deep water formation (Zhang et al., 2022). Moreover, the model resolution may be insufficient to capture potential NADW onset associated with subtle changes in strait geometry.

Model dependency introduces uncertainties and limitations, as emphasized by Model Intercomparison Programs (MIP) such as Deep-Time MIP and Miocene MIP (Burls et al., 2021; Zhang et al., 2022). For example, salinity biases may either trigger or inhibit deep water formation in the regions of interest. Additionally, model physics, including the choice of parametrization for diapycnal mixing, varies across models and tends to modulate the intensity of the global meridional overturning circulation (Zhang et al., 2022). Model resolution also plays a crucial role, as higher resolution allows finer-scale processes and the configuration of straits to be better represented when paleogeography is converted to the ocean grid, impacting both atmospheric and ocean dynamics (Zhang et al., 2022). A multi-model approach would be necessary to determine whether the processes destabilizing the North Atlantic water column are consistent with different models.

Proxy and model SST data show moderate agreement for the early-mid Miocene and mid-late Eocene. The biases observed in both periods, with cooler proxy temperatures relative to models at low latitudes, weaker meridional gradients between subtropical and mid-latitudes, and warmer proxy temperatures relative to models at high latitudes, are common in global climate models (Baatsen et al., 2020; Burls et al., 2021). This bias is crucial for the deep convection process, as the colder modelled high latitudes favour the formation of deep water. However, recent GCM versions incorporating more realistic micro-cloud and aerosol physics have demonstrated improved consistency between modelled and proxy SST data (Baatsen et al., 2020; Hutchinson et al., 2018; Lunt et al., 2007; J. Zhu et al., 2019). Future simulations should incorporate these improvements.

Neodymium (Nd) isotope analysis is a commonly-used method for identifying deep water mass origin through analysis of fish teeth and debris, and can be used to validate the ocean circulation produced by our simulations. Measured ε_{Nd} values from the middle Eocene at Site 689 in the Southern Ocean, in comparison to lower North Atlantic values, suggest a dominance of deep water formation in the Southern Ocean (Via & Thomas, 2006). Similar results were reported by Robinson et al. (2010); Thomas et al. (2014). An alternative hypothesis proposing deep water formation in the North Atlantic to explain

Eocene ε_{Nd} variations remains debated and is not supported by $\delta^{13}C$ data (Scher & Martin, 2004). These findings align with our middle Eocene simulations, which depict a single overturning cell driven solely by deep water formation in the Southern Ocean (Figure 2). In contrast, the averaged radiogenic ε_{Nd} values recorded at Maud Rise during the early Miocene resemble modern Southern Ocean values, suggesting the export of deep water from the North Atlantic (Scher & Martin, 2004), followed by a transition to a modern-like ocean circulation in the middle Miocene (Kirillova et al., 2019). This southern export of NADW is robust in our early Miocene simulation, which shows deep water formation in the North Atlantic and the development of a proto-AMOC cell (Figure 2). However, these reconstructions remain open to interpretation and should be considered with caution. To strengthen the robustness of these conclusions, future work should integrate an explicit neodymium isotope model to enhance model–data comparisons.

In this study, we focused on the processes impacting North Atlantic deep water formation in the Northern Hemisphere, in particular these important for the onset of the deeper branch of the AMOC. However, the Southern Ocean plays a crucial role by bringing intermediate waters to the surface through Ekman transport. The Antarctic Circumpolar Current (ACC), which became more prominent with the opening of the Southern gateways and the initiation of the Antarctic ice sheet (Toumoulin et al., 2020), has been proposed to enhance the upwelling of intermediate waters formed in the North Atlantic (Toggweiler & Samuels, 1995). A logical next step will be to study the role of the Southern Ocean, in order to better constrain its contribution to NADW.

5 Conclusions

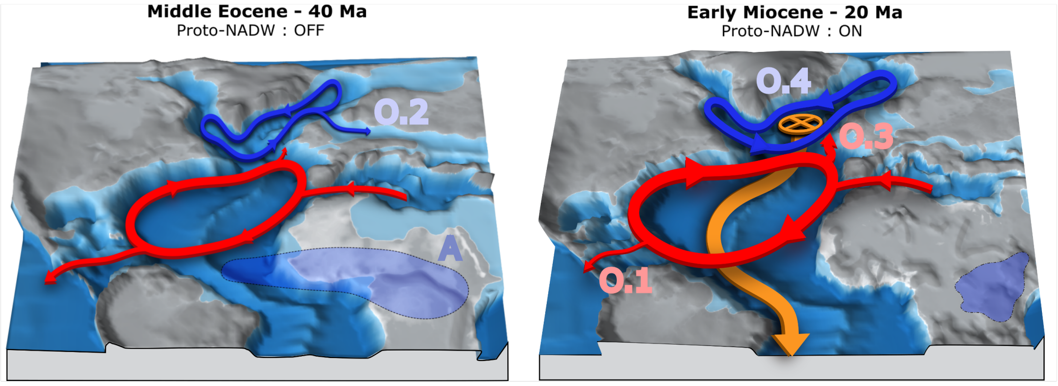

Figure 8. 3D schematic representation of the paleogeographies for the middle Eocene (left) and early Miocene (right), and the processes influencing the stratification of the North Atlantic Ocean and favouring the formation of NADW in the early Miocene simulation (orange). The ocean circulation is shown in red for the subtropical gyre and blue for the subpolar gyre. The salt source and sinks associated with the advection through ocean gateways are represented with arrows, the export to the Pacific (Oceanic processes: O; O.1) and towards the Paratethys (O.2) in the Eocene. The red arrow depicts the northern flux from the subtropical to the subpolar gyre (O.3). The line-width shows the intensity of the subtropical and subpolar gyre (O.4); the African monsoon precipitation (Atmospheric process: A) is represented by the blue shading corresponding to the precipitation isoline of 400 cm/year.

In this paper, we have compared the middle Eocene and early Miocene climates by conducting a complete investigation of the mechanisms favouring NADW formation, with a particular focus on the partitioning between oceanic and atmospheric processes and the quantification of their relative contributions. These processes are summarized as follows (Figure 8):

- In the early Miocene, several oceanic processes contribute to increase the subpolar North Atlantic salinity: The closure of the Central American Seaway (O.1) and the closure of the Polish Strait (O.2) limited salt leakage to the Pacific and Paratethys. Furthermore, the intensified northern salt transport from the subtropical to subpolar gyre in the early Miocene (O.3) increased surface salinity and strengthened the subpolar gyre (O.4). This strengthening was also driven by the widening of the North Atlantic basin and the simulated increase in wind stress. Ultimately, the intensified subpolar gyre helped to promote deep convection through isopycnal uplifting.
- The simulated change in atmospheric dynamics between the middle Eocene and early Miocene shifted the African monsoon eastward and weakened its intensity (A), reducing freshwater input to the Atlantic Ocean and thereby weakening stratification.

Our results suggest that the Eocene paleogeography prevents deep water formation in the Northern Hemisphere, regardless of the atmospheric CO_2 concentration and of the presence of the AIS, but that, together, the processes aforementioned contribute to weakening the stratification of the North Atlantic Ocean and promote the formation of NADW at some point between the middle Eocene and the early Miocene.

Open Research Section

The model outputs used in this article are available here:

- 40 Ma: Toumoulin et al. (2021)
- 20 Ma: Pillot (2022)

The code for the freshwater budget is still under development and is available at this address: "https://github.com/OneAir4Oceans/FreshWaterBudget_GCM"

Acknowledgments
We express our gratitude to P. Sepulchre for his insightful comments and suggestions. We also thank Q. Pillot and A. Toumoulin for providing the simulation data. We are grateful to the OCEAN Institute for funding this work. The simulations used in this work have been performed on the HPC resources of the CEA/TGCC using computing hours provided by GENCI under allocations A0030102212 and A0050102212.

References

Acosta, R. P., Ladant, J.-B., Zhu, J., & Poulsen, C. J. (2022). Evolution of the Atlantic Intertropical Convergence Zone, and the South American and African Monsoons Over the Past 95-Myr and Their Impact on the Tropical Rainforests. *Paleoceanography and Paleoclimatology*, *37*(7), e2021PA004383. doi: 10.1029/2021PA004383

Alexeev, V. A., Langen, P. L., & Bates, J. R. (2005). Polar amplification of surface warming on an aquaplanet in “ghost forcing” experiments without sea ice feedbacks. *Climate Dynamics*, *24*(7-8), 655–666. doi: 10.1007/s00382-005-0018-3

Anagnostou, E., John, E. H., Edgar, K. M., Foster, G. L., Ridgwell, A., Inglis, G. N., … Pearson, P. N. (2016). Changing atmospheric CO2 concentration was the primary driver of early Cenozoic climate. *Nature*, *533*(7603), 380–384. doi: 10.1038/nature17423

Aumont, O., Ethé, C., Tagliabue, A., Bopp, L., & Gehlen, M. (2015). PISCES-v2: an ocean biogeochemical model for carbon and ecosystem studies. *Geoscientific Model Development*, *8*(8), 2465–2513. doi: 10.5194/gmd-8-2465-2015

Baatsen, M., Von Der Heydt, A. S., Huber, M., Kliphuis, M. A., Bijl, P. K., Sluijs, A., & Dijkstra, H. A. (2020). *The middle-to-late Eocene greenhouse climate, modelled using the CESM 1.0.5.* doi: 10.5194/cp-2020-29

Borrelli, C., Cramer, B. S., & Katz, M. E. (2014). Bipolar Atlantic deepwater circulation in the middle-late Eocene: Effects of Southern Ocean gateway openings. *Paleoceanography*, *29*(4), 308–327. doi: 10.1002/2012PA002444

Boyle, P. R., Romans, B. W., Tucholke, B. E., Norris, R. D., Swift, S. A., & Sexton, P. F. (2017). Cenozoic North Atlantic deep circulation history recorded in contourite drifts, offshore Newfoundland, Canada. *Marine Geology*, *385*, 185–203. doi: 10.1016/j.margeo.2016.12.014

Burls, N. J., Bradshaw, C. D., De Boer, A. M., Herold, N., Huber, M., Pound, M., … Zhang, Z. (2021). Simulating Miocene Warmth: Insights From an Opportunistic Multi-Model Ensemble (MioMIP1). *Paleoceanography and Paleoclimatology*, *36*(5), e2020PA004054. doi: 10.1029/2020PA004054

Böning, C. W., Scheinert, M., Dengg, J., Biastoch, A., & Funk, A. (2006). Decadal variability of subpolar gyre transport and its reverberation in the North Atlantic overturning. *Geophysical Research Letters*, *33*(21). doi: 10.1029/2006GL026906

Coxall, H. K., Huck, C. E., Huber, M., Lear, C. H., Legarda-Lisarri, A., O Regan, M., … Backman, J. (2018). Export of nutrient rich Northern Component Water preceded early Oligocene Antarctic glaciation. *Nature Geoscience*, *11*(3), 190–196. doi: 10.1038/s41561-018-0069-9

Crichton, K. A., Ridgwell, A., Lunt, D. J., Farnsworth, A., & Pearson, P. N. (2021). Data-constrained assessment of ocean circulation changes since the middle Miocene in an Earth system model. *Climate of the Past*, *17*(5), 2223–2254. doi: 10.5194/cp-17-2223-2021

Deprez, A., Tesseur, S., Stassen, P., D'haenens, S., Steurbaut, E., King, C., … Speijer, R. P. (2015). Early Eocene environmental development in the northern Peri-Tethys (Aktulagay, Kazakhstan) based on benthic foraminiferal assemblages and stable isotopes (O, C). *Marine Micropaleontology*, *115*, 59–71. doi: 10.1016/j.marmicro.2014.11.003

Doria, G., Royer, D., Wolfe, A., Fox, A., Westgate, J., & Beerling, D. (2011). Declining atmospheric CO2 during the late Middle Eocene climate transition. *American Journal of Science*, *311*. doi: 10.2475/01.2011.03

Engen, O., Faleide, J. I., & Dyreng, T. K. (2008). Opening of the Fram Strait gateway: A review of plate tectonic constraints. *Tectonophysics*, *450*(1), 51–69. doi: 10.1016/j.tecto.2008.01.002

Fedorov, A. M., Bashmachnikov, I. L., Iakovleva, D. A., Kuznetsova, D. A., & Raj, R. P. (2023). Deep convection in the Subpolar Gyre: Do we have enough data to estimate its intensity? *Dynamics of Atmospheres and Oceans*, *101*, 101338. doi: 10.1016/j.dynatmoce.2022.101338

Ferreira, D., Cessi, P., Coxall, H. K., De Boer, A., Dijkstra, H. A., Drijfhout, S. S., … Wills, R. C. (2018). Atlantic-Pacific Asymmetry in Deep Water Formation. *Annual Review of Earth and Planetary Sciences*, *46*(1), 327–352. doi: 10.1146/annurev-earth-082517-010045

Fichefet, T., & Maqueda, M. A. M. (1997). Sensitivity of a global sea ice model to the treatment of ice thermodynamics and dynamics. *Journal of Geophysical Research: Oceans*, *102*(C6), 12609–12646. doi: 10.1029/97JC00480

Fluteau, F., Ramstein, G., & Besse, J. (1999). Simulating the evolution of the Asian and African monsoons during the past 30 Myr using an atmospheric general circulation model. *Journal of Geophysical Research: Atmospheres*, *104*(D10), 11995–12018. doi: 10.1029/1999JD900048

Goldner, A., Herold, N., & Huber, M. (2014). Antarctic glaciation caused ocean circulation changes at the Eocene–Oligocene transition. *Nature*, *511*(7511), 574–577. doi: 10.1038/nature13597

Granot, R., & Dyment, J. (2015). The Cretaceous opening of the South Atlantic Ocean. *Earth and Planetary Science Letters*, *414*, 156–163. doi: https://doi.org/10.1016/j.epsl.2015.01.015

Haug, G. H., Tiedemann, R., Zahn, R., & Ravelo, A. C. (2001, 03). Role of panama uplift on oceanic freshwater balance. *Geology*, *29*(3), 207-210. Retrieved from `https://doi.org/10.1130/0091-7613(2001)029<0207:ROPUOO>2.0.CO;2` doi: 10.1130/0091-7613(2001)029⟨0207:ROPUOO⟩2.0.CO;2

Hauglustaine, D. A., Hourdin, F., Jourdain, L., Filiberti, M.-A., Walters, S., Lamarque, J.-F., & Holland, E. A. (2004). Interactive chemistry in the Laboratoire de Météorologie Dynamique general circulation model: Description and background tropospheric chemistry evaluation: INTERACTIVE CHEMISTRY IN LMDZ. *Journal of Geophysical Research: Atmospheres*, *109*(D4), n/a–n/a. doi: 10.1029/2003JD003957

Herold, N., Huber, M., Müller, R. D., & Seton, M. (2012). Modeling the Miocene climatic optimum: Ocean circulation. *Paleoceanography*, *27*(1). doi: 10.1029/2010PA002041

Hohbein, M. W., Sexton, P. F., & Cartwright, J. A. (2012). Onset of North Atlantic Deep Water production coincident with inception of the Cenozoic global cooling trend. *Geology*, *40*(3), 255–258. doi: 10.1130/G32461.1

Hossain, A., Knorr, G., Lohmann, G., Stärz, M., & Jokat, W. (2020). Simulated Thermohaline Fingerprints in Response to Different Greenland-Scotland Ridge and Fram Strait Subsidence Histories. *Paleoceanography and Paleoclimatology*, *35*(7), e2019PA003842. doi: 10.1029/2019PA003842

Huber, M. (2012). Progress in greenhouse climate modeling. *The Paleontological Society Papers*, *18*, 213–262. doi: 10.1017/S108933260000262X

Huber, M., & Sloan, L. C. (2001). Heat transport, deep waters, and thermal gradients: Coupled simulation of an Eocene greenhouse climate. *Geophysical Research Letters*, *28*(18), 3481–3484. doi: 10.1029/2001GL012943

Huber, M., Sloan, L. C., & Shellito, C. (2003). Early Paleogene oceans and climate: A fully coupled modeling approach using the NCAR CCSM. In *Causes and consequences of globally warm climates in the early Paleogene.* Geological Society of America. doi: 10.1130/0-8137-2369-8.25

Hutchinson, D. K., Coxall, H. K., O Regan, M., Nilsson, J., Caballero, R., & de Boer, A. M. (2019). Arctic closure as a trigger for Atlantic overturning at the Eocene-Oligocene Transition. *Nature Communications*, *10*(1), 3797. doi: 10.1038/s41467-019-11828-z

Hutchinson, D. K., de Boer, A. M., Coxall, H. K., Caballero, R., Nilsson, J., & Baatsen, M. (2018). Climate sensitivity and meridional overturning circulation in the late Eocene using GFDL CM2.1. *Climate of the Past*, *14*(6), 789–810. doi: 10.5194/cp-14-789-2018

Hönisch, B., Royer, D. L., Breecker, D. O., Polissar, P. J., Bowen, G. J., Henehan, M. J., … Zhang, L. (2023). Toward a Cenozoic history of atmospheric CO_2. *Science*, *382*(6675), eadi5177. doi: 10.1126/science.adi5177

Ivanovic, R. F., Valdes, P. J., Flecker, R., & Gutjahr, M. (2014). Modelling global-scale climate impacts of the late Miocene Messinian Salinity Crisis. *Climate of the Past*, *10*(2), 607–622. doi: 10.5194/cp-10-607-2014

Jaramillo, C. A. (2018). *Evolution of the Isthmus of Panama: Biological, Paleoceanographic and Paleoclimatological Implications.* John Wiley & Sons.

Katz, M. E., Cramer, B. S., Toggweiler, J. R., Esmay, G., Liu, C., Miller, K. G., … Wright, J. D. (2011). Impact of Antarctic Circumpolar Current Development on Late Paleogene Ocean Structure. *Science*, *332*(6033), 1076–1079. doi: 10.1126/science.1202122

Kirillova, V., Osborne, A. H., Störling, T., & Frank, M. (2019). Miocene restriction of the Pacific-North Atlantic throughflow strengthened Atlantic overturning circulation. *Nature Communications*, *10*(1), 4025. doi: 10.1038/s41467-019-12034-7

Knies, J., Mattingsdal, R., Fabian, K., Grøsfjeld, K., Baranwal, S., Husum, K., … Gaina, C. (2014). Effect of early Pliocene uplift on late Pliocene cooling in the Arctic–Atlantic gateway. *Earth and Planetary Science Letters*, *387*, 132–144. doi: 10.1016/j.epsl.2013.11.007

Krinner, G., Viovy, N., De Noblet-Ducoudré, N., Ogée, J., Polcher, J., Friedlingstein, P., … Prentice, I. C. (2005). A dynamic global vegetation model for studies of the coupled atmosphere-biosphere system: DVGM FOR COUPLED CLIMATE STUDIES. *Global Biogeochemical Cycles*, *19*(1). doi: 10.1029/2003GB002199

Labails, C., Olivet, J.-L., Aslanian, D., & Roest, W. R. (2010). An alternative early opening scenario for the Central Atlantic Ocean. *Earth and Planetary Science Letters*, *297*(3), 355–368. doi: https://doi.org/10.1016/j.epsl.2010.06.024

Livermore, R., Nankivell, A., Eagles, G., & Morris, P. (2005). Paleogene opening of Drake Passage. *Earth and Planetary Science Letters*, *236*(1), 459–470. doi: 10.1016/j.epsl.2005.03.027

Lozier, M. S., Leadbetter, S., Williams, R. G., Roussenov, V., Reed, M. S. C., & Moore, N. J. (2008). The Spatial Pattern and Mechanisms of Heat-Content Change in the North Atlantic. *Science*, *319*(5864), 800–803. doi: 10.1126/science.1146436

Lunt, D. J., Bragg, F., Chan, W.-L., Hutchinson, D. K., Ladant, J.-B., Morozova, P., … Otto-Bliesner, B. L. (2021). Deepmip: model intercomparison of early eocene climatic optimum (eeco) large-scale climate features and comparison with proxy data. *Climate of the Past*, *17*(1), 203–227. Retrieved from `https://cp.copernicus.org/articles/17/203/2021/` doi: 10.5194/cp-17-203-2021

Lunt, D. J., Valdes, P. J., Haywood, A., & Rutt, I. C. (2007). Closure of the Panama Seaway during the Pliocene: implications for climate and Northern Hemisphere glaciation. *Climate Dynamics*, *30*(1), 1–18. doi: 10.1007/s00382-007-0265-6

Madec, G., Bourdallé-Badie, R., Bouttier, P.-A., Bricaud, C., Bruciaferri, D., Calvert, D., … Vancoppenolle, M. (2016). *NEMO ocean engine.* Notes du Pôle de modélisation de l'Institut Pierre-Simon Laplace (IPSL), Paris, France. doi: 10.5281/zenodo.3248739

Marshall, J., & Schott, F. (1999). Open-ocean convection: Observations, theory, and models. *Reviews of Geophysics*, *37*(1), 1–64. doi: 10.1029/98RG02739

McCarthy, G., Smeed, D., Johns, W., Frajka-Williams, E., Moat, B., Rayner, D., … Bryden, H. (2015). Measuring the atlantic meridional overturning circulation at 26°n. *Progress in Oceanography*, *130*, 91-111. doi: https://doi.org/10.1016/j.pocean.2014.10.006

Miller, K. G., & Tucholke, B. E. (1983). Development of Cenozoic Abyssal Circulation South of the Greenland-Scotland Ridge. In M. H. P. Bott, S. Saxov, M. Talwani, & J. Thiede (Eds.), *Structure and Development of the Greenland-Scotland Ridge: New Methods and Concepts* (pp. 549–589). Boston, MA: Springer US. doi: 10.1007/978-1-4613-3485-9_27

Nisancioglu, K. H., Raymo, M. E., & Stone, P. H. (2003). Reorganization of Miocene deep water circulation in response to the shoaling of the Central American Seaway. *Paleoceanography*, *18*(1). doi: 10.1029/2002PA000767

Palcu, D., & Krijgsman, W. (2021). The dire straits of Paratethys: Gateways to the anoxic giant of Eurasia. *Geological Society London Special Publications*, SP523–2021. doi: 10.1144/SP523-2021-73

Parent, A. M., Chilton, K. D., van Peer, T. E., Bohaty, S. M., Spray, J. F., Scher,

H. D., … Romans, B. W. (2024). Eocene-Oligocene Intensification of the Deep Western Boundary Current in the North Atlantic Ocean. *Paleoceanography and Paleoclimatology*, *39*(4), e2023PA004731. doi: 10.1029/2023PA004731

Pillot, Q. (2022). Evolution of ocean circulation in the North Atlantic Ocean during the Miocene: impact of the Greenland Ice Sheet and the Eastern Tethys Seaway [Dataset]. *Zenodo*. doi: 10.5281/zenodo.6982823

Pillot, Q., Donnadieu, Y., Sarr, A.-C., Ladant, J.-B., & Suchéras-Marx, B. (2022). Evolution of ocean circulation in the north atlantic ocean during the miocene: Impact of the greenland ice sheet and the eastern tethys seaway. *Paleoceanography and Paleoclimatology*, *37*. doi: 10.1029/2022PA004415

Poblete, F., Dupont-Nivet, G., Licht, A., van Hinsbergen, D. J. J., Roperch, P., Mihalynuk, M. G., … Baatsen, M. L. J. (2021). Towards interactive global paleogeographic maps, new reconstructions at 60, 40 and 20 Ma. *Earth-Science Reviews*, *214*, 103508. doi: 10.1016/j.earscirev.2021.103508

Rasser, M., & Harzhauser, M. (2008). Paleogene and Neogene of Central Europe. *Mesozoic and Cenozoic. Geological Society, London*, *2*, 1031–1140.

Robinson, S. A., Murphy, D. P., Vance, D., & Thomas, D. J. (2010). Formation of “Southern Component Water” in the Late Cretaceous: Evidence from Nd-isotopes. *Geology*, *38*(10), 871–874. doi: 10.1130/G31165.1

Sarkar, S., Basak, C., Frank, M., Berndt, C., Huuse, M., Badhani, S., & Bialas, J. (2019). Late Eocene onset of the Proto-Antarctic Circumpolar Current. *Scientific Reports*, *9*(1), 10125. doi: 10.1038/s41598-019-46253-1

Scher, H. D., & Martin, E. E. (2004). Circulation in the Southern Ocean during the Paleogene inferred from neodymium isotopes. *Earth and Planetary Science Letters*, *228*, 391–405. doi: 10.1016/j.epsl.2004.10.016

Scher, H. D., & Martin, E. E. (2008). Oligocene deep water export from the North Atlantic and the development of the Antarctic Circumpolar Current examined with neodymium isotopes. *Paleoceanography*, *23*(1). doi: 10.1029/2006PA001400

Schmittner, A., & Lund, D. C. (2015). Early deglacial atlantic overturning decline and its role in atmospheric co_2 rise inferred from carbon isotopes. *Climate of the Past*, *11*(2), 135–152. doi: 10.5194/cp-11-135-2015

Sepulchre, P., Arsouze, T., Donnadieu, Y., Dutay, J.-C., Jaramillo, C., Le Bras, J., … Waite, A. J. (2014). Consequences of shoaling of the Central American Seaway determined from modeling Nd isotopes. *Paleoceanography*, *29*(3), 176–189. doi: 10.1002/2013PA002501

Sepulchre, P., Caubel, A., Ladant, J.-B., Bopp, L., Boucher, O., Braconnot, P., … Tardif, D. (2020). IPSL-CM5A2 – an Earth system model designed for multi-millennial climate simulations. *Geoscientific Model Development*, *13*(7), 3011–3053. doi: 10.5194/gmd-13-3011-2020

Sosdian, S. M., Greenop, R., Hain, M. P., Foster, G. L., Pearson, P. N., & Lear, C. H. (2018). Constraining the evolution of Neogene ocean carbonate chemistry using the boron isotope pH proxy. *Earth and Planetary Science Letters*, *498*, 362–376. doi: 10.1016/j.epsl.2018.06.017

Spielhagen, R. F., Werner, K., Sørensen, S. A., Zamelczyk, K., Kandiano, E., Budeus, G., … Hald, M. (2011). Enhanced Modern Heat Transfer to the Arctic by Warm Atlantic Water. *Science*, *331*(6016), 450–453. doi: 10.1126/science.1197397

Stickley, C. E., Brinkhuis, H., Schellenberg, S. A., Sluijs, A., Röhl, U., Fuller, M., … Williams, G. L. (2004). Timing and nature of the deepening of the Tasmanian Gateway. *Paleoceanography*, *19*(4). doi: 10.1029/2004PA001022

Straume, E. O., Gaina, C., Medvedev, S., & Nisancioglu, K. H. (2020). Global Cenozoic Paleobathymetry with a focus on the Northern Hemisphere Oceanic Gateways. *Gondwana Research*, *86*, 126–143. doi: 10.1016/j.gr.2020.05.011

Straume, E. O., Nummelin, A., Gaina, C., & Nisancioglu, K. H. (2022). Climate transition at the Eocene–Oligocene influenced by bathymetric changes to the Atlantic–Arctic oceanic gateways. *Proceedings of the National Academy of Sciences*, *119*(17), e2115346119. doi: 10.1073/pnas.2115346119

Stärz, M., Jokat, W., Knorr, G., & Lohmann, G. (2017). Threshold in North Atlantic-Arctic Ocean circulation controlled by the subsidence of the Greenland-Scotland Ridge. *Nature Communications*, *8*(1), 15681. doi: 10.1038/ncomms15681

Talley, L. (2013). Closure of the Global Overturning Circulation Through the Indian, Pacific, and Southern Oceans: Schematics and Transports. *Oceanography*, *26*, 80–97. doi: 10.5670/oceanog.2013.07

Thomas, D. J., Korty, R., Huber, M., Schubert, J. A., & Haines, B. (2014). Nd isotopic structure of the Pacific Ocean 70–30 Ma and numerical evidence for vigorous ocean circulation and ocean heat transport in a greenhouse world. *Paleoceanography*, *29*(5), 454–469. doi: 10.1002/2013PA002535

Toggweiler, J. R., & Samuels, B. (1995). Effect of drake passage on the global thermohaline circulation. *Deep Sea Research Part I: Oceanographic Research Papers*, *42*(4), 477–500. doi: 10.1016/0967-0637(95)00012-U

Toumoulin, A., Donnadieu, Y., Ladant, J.-B., Batenburg, S. J., Poblete, F., & Dupont-Nivet, G. (2020). Quantifying the Effect of the Drake Passage Opening on the Eocene Ocean. *Paleoceanography and Paleoclimatology*, *35*(8), e2020PA003889. doi: 10.1029/2020PA003889

Toumoulin, A., Tardif, D., Donnadieu, Y., Licht, A., Ladant, J.-B., Kunzmann, L., & Dupont-Nivet, G. (2021). Continental temperature seasonality from Eocene Warmhouse to Oligocene Coolhouse [Dataset]. *PANGAEA*. doi: 10.1594/PANGAEA.930422

Toumoulin, A., Tardif, D., Donnadieu, Y., Licht, A., Ladant, J.-B., Kunzmann, L., & Dupont-Nivet, G. (2022). Evolution of continental temperature seasonality from the Eocene greenhouse to the Oligocene icehouse - a model-data comparison. *Climate of the Past*, *18*, 341–362. doi: 10.5194/cp-18-341-2022

Vahlenkamp, M., Niezgodzki, I., De Vleeschouwer, D., Lohmann, G., Bickert, T., & Pälike, H. (2018b). Ocean and climate response to north atlantic seaway changes at the onset of long-term eocene cooling. *Earth and Planetary Science Letters*, *498*, 185-195. Retrieved from `https://www.sciencedirect.com/science/article/pii/S0012821X18303820` doi: https://doi.org/10.1016/j.epsl.2018.06.031

Vahlenkamp, M., Niezgodzki, I., De Vleeschouwer, D., Bickert, T., Harper, D., Kirtland Turner, S., … Pälike, H. (2018a). Astronomically paced changes in deep-water circulation in the western North Atlantic during the middle Eocene. *Earth and Planetary Science Letters*, *484*, 329-340. doi: 10.1016/j.epsl.2017.12.016

Valcke, S. (2013). The OASIS3 coupler: a European climate modelling community software. *Geoscientific Model Development*, *6*(2), 373–388. doi: 10.5194/gmd-6-373-2013

Via, R. K., & Thomas, D. J. (2006, 06). Evolution of atlantic thermohaline circulation: Early oligocene onset of deep-water production in the north atlantic. *Geology*, *34*(6), 441-444. Retrieved from `https://doi.org/10.1130/G22545.1` doi: 10.1130/G22545.1

Yang, S., Galbraith, E., & Palter, J. (2014). Coupled climate impacts of the Drake Passage and the Panama Seaway. *Climate Dynamics*, *43*(1-2), 37–52. doi: 10.1007/s00382-013-1809-6

Zhang, Y., Boer, A. M., Lunt, D. J., Hutchinson, D. K., Ross, P., Flierdt, T., … Huber, M. (2022). Early Eocene Ocean Meridional Overturning Circulation: The Roles of Atmospheric Forcing and Strait Geometry. *Paleoceanography and Paleoclimatology*, *37*(3). doi: 10.1029/2021PA004329

Zhang, Y., Huck, T., Lique, C., Donnadieu, Y., Ladant, J.-B., Rabineau, M., &

Aslanian, D. (2020). Early Eocene vigorous ocean overturning and its contribution to a warm Southern Ocean. *Climate of the Past*, *16*(4), 1263–1283. doi: 10.5194/cp-16-1263-2020

Zhu, C., Liu, Z., Zhang, S., & Wu, L. (2023). Likely accelerated weakening of Atlantic overturning circulation emerges in optimal salinity fingerprint. *Nature Communications*, *14*(1), 1245. doi: 10.1038/s41467-023-36288-4

Zhu, C., Zhang, Z., Zhu, C., & Zhang, J. (2023). Potential Role of Mid-Latitude Seaway on Early Paleogene Atlantic Overturning Circulation. *Geophysical Research Letters*, *50*(10), e2023GL102794. doi: 10.1029/2023GL102794

Zhu, J., Poulsen, C. J., & Tierney, J. E. (2019). Simulation of Eocene extreme warmth and high climate sensitivity through cloud feedbacks. *Science Advances*, *5*(9), eaax1874. doi: 10.1126/sciadv.aax1874